

Prediction of strong dichroism induced by x-rays carrying orbital momentum

Michel van Veenendaal^{1,2} and Ian McNulty²

¹*Dept. of Physics, Northern Illinois University, De Kalb, Illinois 60115*

²*Advanced Photon Source, Argonne National Laboratory,
9700 South Cass Avenue, Argonne, Illinois 60439*

(Dated: January 16, 2007)

We predict the presence of strong dichroic effects induced by x-ray beams carrying orbital angular momentum (OAM). Taking the difference between spectra obtained with positive and negative OAM states allows the separation of quadrupolar from dipolar transitions at, e.g., the transition-metal K edges, enabling the study of the unoccupied states in the absence of strong core-hole effects. We study the dependence of OAM-induced x-ray dichroism on different polarization vectors and derive sum rules relating the integrated intensity to ground-state hole densities. Calculations of spectral line shapes for cuprates, manganites, and ruthenates confirm the strong OAM-induced dichroism and indicate the potential of this new spectroscopy in the fields of orbital physics and magnetism.

PACS numbers: 78.70.Dm, 78.20.Fm

–*Introduction.* The field of singular optics has grown rapidly in the last 15 years after the demonstration that beams with shaped profiles carry orbital angular momentum (OAM) [1]. So far, the focus has been on optical vortex beams in the visible region, which have been used for manipulation of molecules and nanoparticles [2], and the possible detection of faint astronomical objects [3]. The interaction between OAM-carrying light and matter was studied for molecules in Laguerre-Gaussian and Bessel shaped laser modes [4–6]. More recently, the possibility of creating phase singularities with x-rays was demonstrated [7, 8]. In this Letter, we study absorption from core states using singular x-ray beams and predict the presence of significant dichroic effects induced by a reversal of the orbital angular momentum of the beam at a fixed polarization of the x-rays. Since core-level resonances are dominated by dipolar and quadrupolar transitions, the interpretation of these experiments is expected to be more straightforward than OAM-induced spectroscopy in the visible region.

–*Theory.* Inside the waist w of a singular x-ray beam, the spacial dependence of the vector potential for azimuthal mode index n , frequency ω , and the wavevector \mathbf{k} along the z axis, is given by $\mathbf{A}_n(\mathbf{r}) = \hat{\mathbf{e}}A_n\left(\frac{\rho}{w}\right)^{|n|}e^{in\varphi+ikz}$ [1, 4–6], where $\hat{\mathbf{e}}$ is the polarization vector, ρ the distance to the center of the beam, φ the azimuthal phase, and A_n the strength of the vector potential. X-ray spectroscopic line shapes are dominated by dipolar and quadrupolar transitions from the core level into the valence shell. We restrict ourselves here to $n = \pm 1$, which are the most relevant for quadrupolar transitions and use the approximation $e^{ikz} \cong 1$ [4–6]. The vector potential in this limit is $\mathbf{A}_{\pm 1}(\mathbf{r}) = \hat{\mathbf{e}}A_{\pm 1}\frac{\rho}{w}e^{\pm i\varphi}$. For electronic transitions, it is more convenient to express this in the spherical tensors $r_q^{(k)} = r^k\sqrt{4\pi/(2k+1)}Y_{kq}(\theta, \varphi)$, where Y_{kq} is a spherical harmonic. This gives $\mathbf{A}_{\pm 1} = \mp\hat{\mathbf{e}}A_{\pm 1}r_{\pm 1}^{(1)}/w$. To study the interaction between light and matter, we evaluate the matrix elements $\langle f|\frac{e}{m}\mathbf{p}\cdot\mathbf{A}(\mathbf{R}+\mathbf{r})|g\rangle \cong i\omega e\langle f|\mathbf{r}\cdot\mathbf{A}(\mathbf{R}+\mathbf{r})|g\rangle$, where g and f denote ground and

final states, respectively; \mathbf{R} is the position of the atom with respect to the center of the beam; the photon energy $\hbar\omega = E_f - E_g$. The vector potential for an atom at \mathbf{R} is $i\omega\mathbf{A}_{\pm 1}(\mathbf{R}+\mathbf{r}) = \mp\hat{\mathbf{e}}E_{\pm 1}(R_{\pm 1}^{(1)} + r_{\pm 1}^{(1)})/w$ where $E_n = i\omega A_n$ is the electric field strength. For a particular component \hat{e}_q of the polarization vector, we have two types of transitions: dipolar transitions $R_{\pm 1}^{(1)}\langle f|r_q^{(1)}|g\rangle$ due to the off-axis position of the atom and quadrupolar transitions $\langle f|r_{\pm 1}^{(1)}r_q^{(1)}|g\rangle = a_{q\pm 1}\langle f|r_{q\pm 1}^{(2)}|g\rangle$ due to the radial dependence of the singular x-ray beam. The coefficients between the spherical tensors of different rank, $a_{\pm 1} = 1/\sqrt{3}$, $a_{\pm 2} = \sqrt{2/3}$, and $a_0 = 1/3$, can be derived from the relationships between the spherical harmonics. The absorption for an atom at a site \mathbf{R} is then

$$I_{\pm 1}(\hat{\mathbf{e}}, \omega, \mathbf{R}) = \frac{e^2 E_{\pm 1}^2}{w^2} \sum_{f q' q} \hat{e}_{q'} \hat{e}_q^* |\rho_R^2 M_{1q'}^{f*} M_{1q}^f \pm (R_{\mp 1}^{(1)} a_{q\pm 1} M_{1q'}^{f*} M_{2,q\pm 1}^f - R_{\pm 1}^{(1)} a_{q'\pm 1} M_{2,q'\pm 1}^{f*} M_{1q}^f) + a_{q'\pm 1} a_{q\pm 1} M_{2,q'\pm 1}^{f*} M_{2,q\pm 1}^f|, \quad (1)$$

where $M_{kq}^f = \langle f|r_q^{(k)}|g\rangle$, ρ_R is the distance of the atom to the center of the beam. We have three different terms. The first term is dipolar and independent of the winding number. The dipole-quadrupole interference terms between the parentheses only contribute when the local inversion symmetry is broken. The last term gives rise to quadrupolar transitions. In the remainder, we discuss the situation for symmetries relevant for most transition-metal compounds, i.e. with inversion symmetry and a sufficiently high symmetry (e.g. SO_2 , O_h , or D_{4h}), where the cross terms $q' \neq q$ are zero. The expression then reduces to

$$I_{\pm 1}(\hat{\mathbf{e}}, \omega) = \pi e^2 E_{\pm 1}^2 \sum_{fq} |\hat{e}_q|^2 \left(\frac{w^2}{2} |M_{1q}^f|^2 + a_{q\pm 1}^2 |M_{2,q\pm 1}^f|^2 \right),$$

where we have performed an integration over the waist $\rho_R \leq w$ of the singular beam.

The OAM dichroic signal I_d for a particular polarization vector is obtained from the difference between $n = 1$ and -1 , $I_d(\hat{\mathbf{e}}, \omega) = I_1(\hat{\mathbf{e}}, \omega) - I_{-1}(\hat{\mathbf{e}}, \omega)$, with equal intensities normalized to unity, $\pi e^2 E_{\pm 1} \equiv 1$. Since the dipolar term is independent on the OAM, it cancels and only the quadrupolar terms remain. Herein lies the strength of OAM x-ray dichroism. For example, for transition-metal compounds, one would like to probe the $3d$ states, but, for x-ray absorption at the transition-metal K edge, the quadrupolar $1s \rightarrow 3d$ transitions are generally obscured by the presence of the strong dipolar $1s \rightarrow 4p$ transitions. Obviously, direct transitions into the $3d$ shell occur at the transition-metal L edges, but here the interpretation is often complicated by the presence of strong core-hole effects, such as the large spin-orbit coupling and Coulomb multiplet interactions between the core and valence shell. OAM-induced x-ray dichroism therefore provides unique insights into the unoccupied $3d$ projected density of states. Experiments are also possible at, e.g., the rare-earth L -edges, but core-hole effects are present.

It is insightful to compare the quadrupolar transition induced by the singular x-ray beam with the usual electric quadrupole transitions for a plane wave. In the latter, quadrupole terms arise from higher-order contributions in the expansion of the plane wave $e^{i\mathbf{k}\cdot\mathbf{r}} \cong 1 + i\mathbf{k}\cdot\mathbf{r}$, and the relative scaling between the dipolar and quadrupolar transitions is $k/2\sqrt{5}$. Quadrupolar transitions in singular x-ray beams arise from the radial dependence $\frac{r_{\pm 1}}{w}$ of the vector potential and the relative scaling between dipolar and quadrupolar transitions is inversely proportional to the waist size of the beam $\sqrt{2}/w$. Beam waist sizes of 25 Å have been demonstrated [9] and 10 Å appears feasible. This makes the relative scaling of the quadrupolar to dipolar terms about a factor 50 smaller for the singular beams compared to regular quadrupolar transitions. On the other hand, for the dichroic signal, the only contribution is expected to come from the quadrupolar term from the singular nature of the x-ray beam, whereas dipolar terms should give no contribution. In addition, for transition-metal K edges the transition are expected to occur in the pre-edge region which occurs about 5-10 eV lower in energy than the $1s \rightarrow 4p$ edge, further distinguishing it from the dipolar signal. The experiment gives for circular polarization vectors $\hat{\mathbf{e}}_{\pm 1}$

$$I_d(\hat{\mathbf{e}}_{\pm 1}, \omega) = \pm \frac{2}{3} I_{2,\pm 2}(\omega) \mp \frac{1}{9} I_{20}(\omega), \quad (2)$$

where the spectrum for the component q of $r_q^{(k)}$ is given by $I_{kq}(\omega) = \sum_f |M_{kq}^f|^2 \delta(E_f - E_g - \hbar\omega)$, with $q = -2, -1, 0, 1, 2$. At the transition-metal K -edge ($1s \rightarrow 3d$), the transition matrix elements are, in second quantization, $\langle d|r_q^{(2)}|s\rangle = \frac{1}{\sqrt{5}}(d||r^{(2)}||s) \sum_{\sigma} \langle d|d_{q\sigma}^{\dagger} s_{0\sigma}|s\rangle$, where $d_{m\sigma}^{\dagger}$ and $s_{m\sigma}^{\dagger}$ create an electron with orbital momentum m and spin $\sigma = \pm \frac{1}{2}$ in the $3d$ and $1s$ shells, respectively; For clarity, the reduced matrix element $(d||r^{(2)}||s)$, which is a constant scaling factor, will be set to unity. The transition matrix elements are a simple scaling fac-

tor. Therefore, the transitions are $1s \rightarrow xy, x^2 - y^2$ and $1s \rightarrow 3z^2 - r^2$ for $q = \pm 2$ and $q = 0$, respectively. This makes this technique very sensitive changes between in-plane and out-of-plane electron distributions. It shares some similarities with linear dichroism, which can also be used to determine the orientation of the charge density, in particular for simple systems such as Cu compounds [10]. Linear dichroism for dipolar transitions, however, measures $I_{11}(\omega) - 2I_{10}(\omega) - I_{1,-1}(\omega)$. Since the orbital angular momentum of the $2p$ core hole is $m = -1, 0, 1$, all $3d$ orbitals can be reached in this experiment. In addition, there is an increased complexity due to the dipole matrix elements and core-valence shell interaction. Linear dichroism using quadrupolar transition has a complicated angular dependence. The transition operator is given by $\langle f|\hat{\mathbf{e}}\cdot\mathbf{r}\hat{\mathbf{k}}\cdot\mathbf{r}|g\rangle$. For example, with the k -vector along the z -axis and linearly polarized light, transitions $1s \rightarrow yz, zx$ are made. However, for grazing incidence, the role of $\hat{\mathbf{e}}$ and $\hat{\mathbf{k}}$ is interchanged and the same transitions are made. The OAM-induced dichroism is more straightforward to interpret as will be demonstrated by several applications below. Finally, for OAM-induced dichroism using linearly polarized light (x or y polarization), we have $I_d(\hat{\mathbf{e}}_{x/y}, \omega) = \frac{1}{3}[I_{22}(\omega) - I_{2,-2}(\omega)]$.

–*Sum rules.* Sum rules that relate the integrated intensity of a spectrum to ground-state expectation values of operators, such as the number of holes and the orbital moment, have played an important role in the development of x-ray magnetic dichroism [11]. The integrated intensities are

$$I_d(\hat{\mathbf{e}}_{\pm 1}) = \int I_d(\hat{\mathbf{e}}_{\pm 1}, \omega) d\omega = \pm \frac{2}{15} \langle n_{\pm 2} \rangle \mp \frac{1}{45} \langle n_0 \rangle, \quad (3)$$

where the integration goes over the $1s \rightarrow 3d$ transitions; $\langle n_m \rangle$ is the hole density in the $3d$ orbital with angular momentum m . For transition-metal compounds, it is often more convenient to use real orbitals instead of atomic-like orbitals, giving

$$I_d(\hat{\mathbf{e}}_{\pm 1}) = \pm \frac{1}{15} (\langle n_{x^2-y^2} \rangle + \langle n_{xy} \rangle) \mp \frac{1}{45} \langle n_{3z^2-r^2} \rangle + \frac{i}{15} \langle d_{x^2-y^2} d_{xy}^{\dagger} - d_{xy} d_{x^2-y^2}^{\dagger} \rangle. \quad (4)$$

When using linearly polarized light, the sum rule is

$$I_d(\hat{\mathbf{e}}_{x/y}) = \frac{1}{15} (\langle n_2 \rangle - \langle n_{-2} \rangle) = \frac{i}{15} \langle d_{x^2-y^2} d_{xy}^{\dagger} - d_{xy} d_{x^2-y^2}^{\dagger} \rangle. \quad (5)$$

–*Applications: Cuprates.* To obtain a better understanding of this new spectroscopy, let us consider the simple system of a divalent copper atom. In spherical symmetry with a magnetic field along the z axis (SO_2), the ground state has a hole in the orbital with $m = -2$ and $\sigma = -\frac{1}{2}$, see the bottom inset in Fig. 1(a). Transitions can only be made for $n + q = -2$, requiring $q = -1$ (\mathbf{e}_{-1}) and winding number $n = -1$.

The integrated intensity is $I_d(\hat{e}_{-1}) \sim -\frac{2}{15} \langle n_{-2} \rangle$. The absorption for e_{-1} is zero and for linear polarization, the average of left and right circularly polarized light is obtained. The spectra change significantly for a copper atom in a local D_{4h} symmetry, see Fig. 1(b), corresponding to a Cu atom surrounded by an octahedron of ligand atoms elongated in the z -direction, a typical situation in cuprates. In the absence of $3d$ spin-orbit coupling, the ground state is a hole in the $x^2 - y^2$ orbital, and the spectra for left and right circularly polarized light are equal with an integrated intensity $I_d(\hat{e}_{\pm 1}) = \pm \frac{1}{15} \langle n_{x^2-y^2} \rangle$. However, in the presence of the $3d$ spin-orbit coupling of strength $\zeta = 0.13$ eV the ground state is $|g\rangle = |x^2 - y^2 \downarrow\rangle - \frac{i\zeta}{E_{xy}} |xy \downarrow\rangle + \frac{\zeta}{2E_{yz/zx}} (i|yz \uparrow\rangle + |zx \uparrow\rangle)$, to lowest order in ζ with E_{xy} and $E_{yz/zx}$ the on-site energy for a hole in the xy and yz/zx orbitals, respectively, relative to a hole in the $x^2 - y^2$ orbital, where, for Fig. 1(b), $E_{xy} = E_{yz/zx} = 1.5$ eV. We obtain for the hole densities $\langle n_{\mp 2} \rangle = \frac{1}{2} (1 \pm \zeta/E_{xy})^2$. For linearly polarized light, the integrated intensity is significantly smaller, $\frac{i}{15} \langle d_{x^2-y^2} d_{xy}^\dagger - d_{xy} d_{x^2-y^2}^\dagger \rangle = -2\zeta/E_{xy}$. In an antiferromagnetic system, the spin-orbit related part cancels.

–*Manganites*. As described in the previous sections, OAM-induced dichroism is sensitive to relative changes in the occupancy of the e_g orbitals $3z^2 - r^2$ and $x^2 - y^2$. This characteristic can be beneficial when studying, e.g. manganites where the interplay between the e_g orbitals plays a crucial role. Manganites show a strong magnetoresistance [12], that was explained by the double-exchange between the Mn t_{2g} core spins through the delocalized e_g electrons [13]. However, the presence of a strong dynamic Jahn-Teller coupling is often considered necessary to explain a change in conductivity of several orders of magnitude [14]. These Jahn-Teller distortions have different orientations and have been studied with x-ray spectroscopy, such as x-ray magnetic linear dichroism [15]. However, the large core-hole spin-orbit coupling and the $2p$ - $3d$ Coulomb multiplets [15] complicate the distinction between the different orbital orientations. The $1s$ - $3d$ exchange interaction is only 0.06 eV [16], and

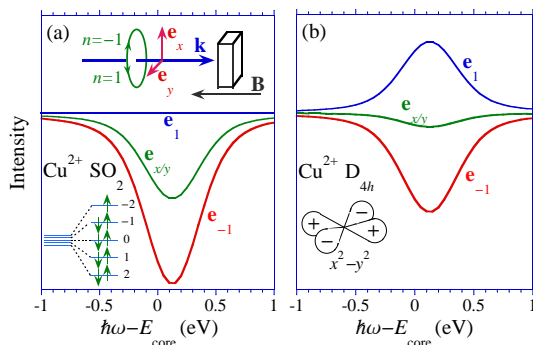


FIG. 1: (color online) (a) The dichroic OAM signal for circular (e_1 and e_{-1}) and linear ($e_{x/y}$) polarization of the incoming x-rays for a divalent copper ion in spherical symmetry with a magnetic field along the z axis. (b) The same, but for a Cu^{2+} atom in a crystal field with D_{4h} symmetry.

the OAM-induced x-ray dichroism reflects more closely the unoccupied density of states. Figure 2 shows the difference in OAM x-ray dichroic spectral lines shapes for $S = 2$ ground states with $t_{2g}^3 \uparrow 3z^2 - r^2 \uparrow$ and $t_{2g}^3 \uparrow x^2 - y^2 \uparrow$ configurations. A clear distinction is observed at the absorption edge for the $t_{2g}^3 e_g^2 \uparrow$ ($S = 5/2$) final state. For the $t_{2g}^3 \uparrow 3z^2 - r^2 \uparrow$ ground state, excitations are made into the $x^2 - y^2 \uparrow$ orbital. Since $x^2 - y^2$ is a linear combination of $m = 2$ and -2 atomic-like orbitals, the peak is positive. For the $t_{2g}^3 \uparrow x^2 - y^2 \uparrow$ ground state, a high-spin state is created by adding a $3z^2 - r^2 \uparrow$ ($m = 0$) electron, and the peak intensity in the dichroism is negative. The spectral features more than 2 eV above the absorption edge are $S = 3/2$ multiplet states. At energies greater than 6 eV above the edge, the dichroic signal is opposite to that just above the edge. These multiplets contain a $3z^2 - r^2 \uparrow 3z^2 - r^2 \downarrow$ or $x^2 - y^2 \uparrow x^2 - y^2 \downarrow$ configuration, which is energetically unfavorable.

–*Ruthenates*. Since $I_d(\hat{e}, \omega)$ includes $1s \rightarrow xy$ transitions, but not $1s \rightarrow yz/zx$, changes in in-plane/out-of-plane electron distributions can also be studied for the t_{2g} orbitals. A system where strong changes in the t_{2g} occupations have been observed are the ruthenates, e.g. Ca_2RuO_4 [17]. Calculations are done for a RuO_6 cluster with hybridization matrix elements ($pd\pi$) = -0.45 ($pd\sigma$) = 1.4 eV, a charge-transfer energy of 4 eV, and an on-site Coulomb interaction of 3 eV. Atomic spin-orbit coupling and Coulomb multiplet parameters are used [16]. The strong crystal-field splitting consisting of a point-charge crystal field, which we take 1.5 eV, and the strong hybridization results in a low-spin t_{2g}^4 ground state. Since we are interested in the effect of the in-plane versus out-of-plane t_{2g} occupation on the OAM x-ray dichroism, we introduce a splitting between the xy and yz/zx orbitals, $E_{yz/zx} - E_{xy}$, to vary the relative occupations. Figure 3(a) shows the OAM x-ray dichroism for \hat{e}_1 . The spectra for \hat{e}_{-1} are very similar. Due

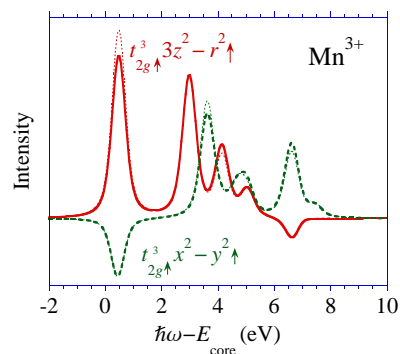


FIG. 2: (color online) OAM x-ray dichroism spectra for a Mn^{3+} ion. The polarization vectors are \hat{e}_1 (solid and dashed) and \hat{e}_{-1} (dotted). For a $t_{2g}^3 \uparrow 3z^2 - r^2 \uparrow$ ground state (red solid), we observe close to the absorption edge $1s \rightarrow x^2 - y^2 \uparrow$ excitations leading to a large positive peak. For a $t_{2g}^3 \uparrow x^2 - y^2 \uparrow$ ground state (green dashed), the excitations close to the edge are into the $3z^2 - r^2 \uparrow$ states and therefore show up as a negative peak in the OAM-induced x-ray dichroism.

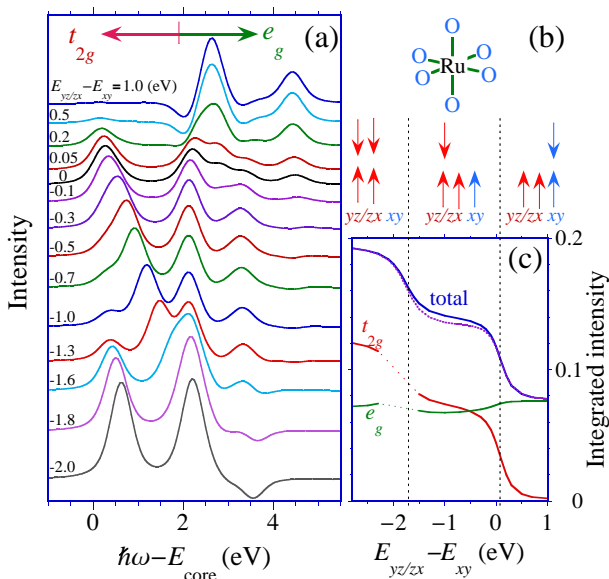


FIG. 3: (color online) (a) OAM x-ray dichroism for ruthenates calculated for a RuO₆ cluster, see (b), for a splitting of the t_{2g} orbitals given by $E_{yz/zx} - E_{xy}$ as given in the Figure. (c) The integrated intensity of the spectrum as a function of $E_{yz/zx} - E_{xy}$. The solid line (blue, solid) gives the total integrated intensity for an incoming polarization vector \hat{e}_1 and \hat{e}_{-1} (purple, dotted). The curves indicated t_{2g} (red) and e_g (green) give the integrated intensities for the low-energy states (< 2 eV) and the high-energy states (> 2 eV), respectively, only OAM for \hat{e}_1 is shown. The dotted part indicates the region where the low- and high-energy states are difficult to separate.

to the large crystal-field splitting, we can often clearly separate the excitations into the xy orbitals (< 2 eV) and the e_g orbitals (> 2 eV). Figure 3(c) shows the integrated intensities as a function of $E_{yz/zx} - E_{xy}$. We see a decrease of the total intensity, see Fig. 3(c). By separating the integrated intensity into low- and high-energy regions, we see that the change in intensity is mainly

a result of the decrease in intensity in the low-energy region related to $1s \rightarrow xy$ excitations. We can distinguish three plateaus, corresponding to ground states with predominantly $yz\uparrow yz\downarrow zx\uparrow zx\downarrow$ (2 xy holes, with an integrated intensity of $\frac{2}{15}$), $yz\uparrow zx\uparrow (yz/zx)\downarrow xy\uparrow$ (1 xy hole), and $(yz/zx)\uparrow (yz/zx)\downarrow xy\uparrow xy\downarrow$ (no xy holes) character, see Fig. 3(b). The integrated intensity basically follows the xy hole density. The transitions between the different ground states is smooth due to the $4d$ spin-orbit coupling.

– *Conclusions.* We have shown the possibility of performing quadrupolar x-ray dichroism experiments using x-rays carrying orbital angular momentum. Taking the difference between negative and positive OAM states removes the OAM-independent electric multipole transitions and dipolar transitions related to the off-axis position of the beam. The signal of the quadrupolar OAM-induced signal can be enhanced with respect to the other contributions by the use of x-ray OAM beams approaching the scale of atomic orbital dimensions. Diffractive optics for focusing intense coherent x-ray beams to the nanometer scale have been demonstrated [9], and focusing singular x-ray optics along similar principles are feasible [18]. OAM-induced x-ray dichroism provides a unique way to study the electron-addition states close to the Fermi level in the absence of core-hole spin-orbit splitting and strong core-valence multiplet interactions. In particular, the spectral line shape is very sensitive to changes in orbital occupancies, such as in-plane/out-of-plane redistributions of electron densities. Finally, we suggest that this approach might be applied to study x-ray OAM-induced dichroism effects in resonant x-ray scattering experiments.

Discussions with Andreas Menzel and Serkan Erdin are acknowledged. This work was supported by the U.S. Department of Energy (DOE), DE-FG02-03ER46097, and NIU’s Institute for Nanoscience, Engineering, and Technology under a grant from the U.S. Department of Education. Work at Argonne National Laboratory was supported by the U.S. DOE, Office of Science, Office of Basic Energy Sciences, under contract DE-AC02-06CH11357.

-
- [1] L. Allen *et al.*, Phys. Rev. A **45**, 8185 (1992).
[2] For a review, see D. G. Grier, Nature **424**, 810 (2003).
[3] J. H. Lee, G. Foo, E. G. Johnson, and G. A. Swartzlander, Jr. Phys. Rev. Lett. **97**, 053901 (2006).
[4] M. Babiker *et al.*, Phys. Rev. Lett. **89**, 143601 (2002).
[5] A. Alexandrescu, E. Di Fabrizio, and D. Cojoc, J. Opt. B: Quantum Semiclass. Opt. **7**, 87 (2005).
[6] A. Alexandrescu, D. Cojoc, and E. Di Fabrizio, Phys. Rev. Lett. **96**, 243001 (2006).
[7] A. G. Peele *et al.*, Opt. Lett. **27**, 1752 (2002); A. G. Peele *et al.*, J. Opt. Soc. Am. A **21**, 1575 (2004).
[8] I. McNulty, S. Rehbein, S. Eisebitt, A. Menzel, C. Günther, and F. Senf, Appl. Phys. Lett., in press.
[9] W. Chao *et al.*, Nature **435**, 1210 (2005); H. C. Kang *et al.*, Phys. Rev. Lett. **96**, 127401 (2006).
[10] C. T. Chen *et al.*, Phys. Rev. Lett. **68**, 2543 (1992).
[11] B. T. Thole, P. Carra, F. Sette, and G. van der Laan, Phys. Rev. Lett. **68**, 1943 (1992); P. Carra, B. T. Thole, M. Altarelli, and X. Wang, *ibid.* **70**, 694 (1993).
[12] For a review, see M. B. Salamon and M. Jaime, Rev. Mod. Phys. **73**, 583 (2001).
[13] C. Zener, Phys. Rev. **82**, 403 (1951); P. W. Anderson and H. Hasegawa, Phys. Rev. **100**, 675 (1955).
[14] A. J. Millis, P. B. Littlewood, and B. I. Shraiman, Phys. Rev. Lett. **74**, 5144 (1995).
[15] D. J. Huang *et al.*, Phys. Rev. Lett. **92**, 087202 (2004).
[16] R. D. Cowan, *The Theory of Atomic Spectra* (University of California Press, Berkeley, 1981).
[17] T. Mizokawa *et al.*, Phys. Rev. Lett. **87**, 077202 (2001).
[18] D. Cojoc *et al.*, Microelectronic Engineering **83**, 1360

(2006).